Visualizing Interactions Between Solar Photovoltaic Farms and the Atmospheric Boundary Layer

Tushar M. Athawale*
tushar.athawale@sci.utah.edu
University of Utah
Salt Lake City, Utah, USA

Brooke J. Stanislawski*
brooke.stanislawski@utah.edu
University of Utah
Salt Lake City, Utah, USA

Sudhanshu Sane
ssane@sci.utah.edu
University of Utah
Salt Lake City, Utah, USA

Chris R. Johnson
crj@sci.utah.edu
University of Utah
Salt Lake City, Utah, USA

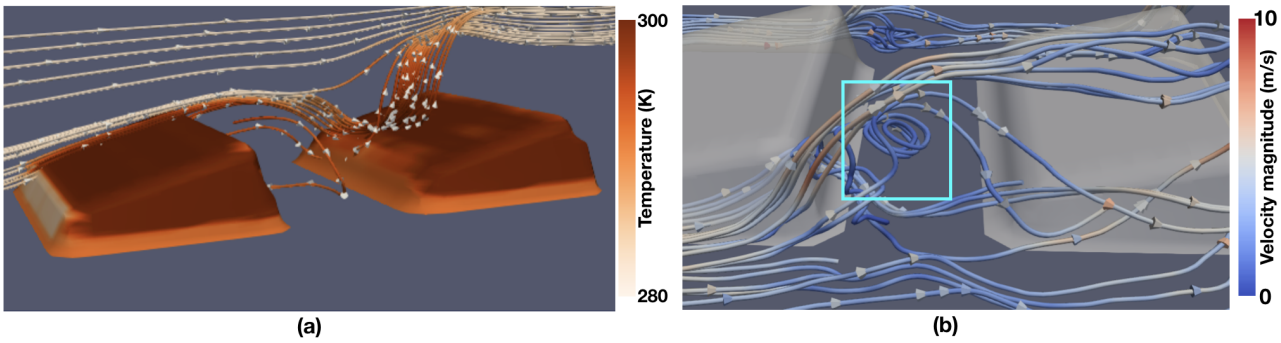

Figure 1: Visualization of the air flow near solar photovoltaic modules. (a) Heat transfer from solar panels to air particles. (b) Visualization of the eddy formation, as indicated by the cyan box.

ABSTRACT

The efficiency of solar panels depends on the operating temperature. As the panel temperature rises, efficiency drops. Thus, the solar energy community aims to understand the factors that influence the operating temperature, which include wind speed, wind direction, turbulence, ambient temperature, mounting configuration, and solar cell material. We use high-resolution numerical simulations to model the flow and thermal behavior of idealized solar farms. Because these simulations model such complex behavior, advanced visualization techniques are needed to investigate and understand the results. Here, we present advanced 3D visualizations of numerical simulation results to illustrate the flow and heat transport in an idealized solar farm. The findings can be used to understand how flow behavior influences module temperatures, and vice versa.

*Both authors contributed equally to this research.

EnergyVis '21, June 28, 2021, Torino, Italy (virtual)

ACM ISBN 978-1-4503-XXXX-X/18/06…$15.00
https://doi.org/10.1145/3447555.3466599

CCS CONCEPTS

• **Human-centered computing** → **Scientific visualization**; **Visualization toolkits**.

KEYWORDS

Solar panels, heat transfer, temperature, flow, large-eddy simulation

ACM Reference Format:
Tushar M. Athawale, Brooke J. Stanislawski, Sudhanshu Sane, and Chris R. Johnson. 2021. Visualizing Interactions Between Solar Photovoltaic Farms and the Atmospheric Boundary Layer. In *EnergyVis '21: 2nd Workshop on Energy Data Visualization, June 28, 2021, Torino, Italy (virtual).* ACM, New York, NY, USA, 5 pages. https://doi.org/10.1145/3447555.3466599

1 INTRODUCTION

The temperature of solar panels affects their efficiency. Commonly installed mono- and polycrystalline solar cells experience an efficiency loss of 0.1% to 0.5% K^{-1} for each degree increase [5]. Considering this trend, we study the flow and heat transport in solar farms by performing simulations of the interaction of solar farms with the atmospheric boundary layer (ABL) and deriving 3D visualizations to interpret the simulation data.

We perform numerical simulations using a large-eddy simulation (LES) model [3, 13, 15]. In our context, the LES model is a thermally-coupled numerical model for solar farms that resolves the ABL flow and accounts for the thermal exchanges between the

solar farm and the surrounding flow. This LES model solves the continuity equation and the 3D filtered incompressible Navier-Stokes equation for momentum, and the advection-diffusion equation for temperature. In this work, u, v, and w denote the flow velocity in x, y, and z, which represent the streamwise, spanwise, and vertical directions, respectively. The flow is driven by a constant pressure gradient force in the streamwise direction. The idealized solar farm topography is represented by the Immersed Boundary Method [13, 15].

We simulate the temperature, flow, and heat flux fields of an idealized solar farm in a domain of size 2π km $\times$ 2π km $\times$ 1 km that is discretized into a $64 \times 64 \times 60$ rectilinear grid for a duration of 185.4 minutes and temporal resolution of 500,000 time steps. Fig. 2 illustrates 1D and 2D plots (similar to those in [11, 17]) of the LES variables, in which distances are normalized by $z_i = 1km$, the height of the ABL.

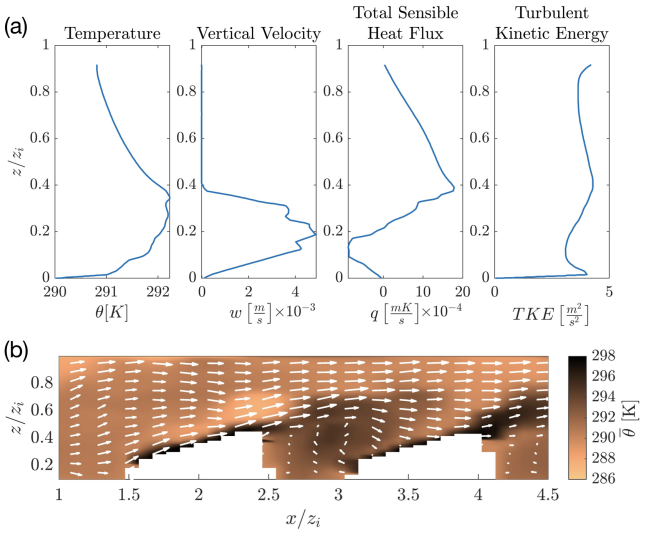

Figure 2: Illustration of (a) 1D vertical profiles generated by averaging x-y plane values over the last 5.5 seconds of simulation. (b) 2D slice depicting the instantaneous fields of temperature θ and velocity vectors at 183.24 minutes.

Although 1D/2D visualizations are useful and necessary, advanced 3D visualizations can strongly reinforce 1D/2D visualizations and uncover new insights into the complex flow in large-scale simulations. Specifically, advanced 3D visualizations of data can play three key roles: enhance communication by improving the presentation of the physical phenomena of interest, aid the exploration process for new insight, and support model verification by revealing anomalies and errors in the results during the development stage.

Using the results from high-fidelity numerical simulations, this work aims to visualize physical phenomena, such as velocity, temperature, heat flux, and the relationships among these variables, through scalar- and vector-field visualization techniques in ParaView [1] and VisIt [4]. ParaView and VisIt are parallel visualization software systems that enable efficient rendering of large-scale complex datasets using the Visualization Toolkit (VTK) libraries [14]. Our proposed visualizations aim to answer the following questions:

(1) Where are the hot and cold spots on a solar panel and how do they change with time?
(2) How does the air temperature respond to the heat source from the solar panels in time?
(3) Where in the domain are the flow eddies, as well as the highest and lowest flow velocities observed?
(4) What relationships between the flow (u, v, w) and heat transfer are observed?

We design questions relevant to operating temperatures (Q. 1-2) and flow patterns (Q. 3-4) since their study is important in the design of solar photovoltaic systems [5, 17].

2 VISUALIZATIONS OF FLOW AND HEAT TRANSPORT IN SOLAR FARMS

We now present the visualization results in Sec. 2.1- 2.4 to address the questions 1-4, respectively, proposed in the Introduction.

2.1 Visualization of the Temperature Field on Solar Panel Surfaces

Fig. 3 illustrates the temperature statistics visualization to gain insight into relatively hot and cool positions on solar panels. Specifically, we visualize minimum, maximum, mean, and standard deviation of temperatures at each position on the solar panel surfaces over the last 11.1 seconds of the simulation. The red regions in the mean visualization (Fig. 3c) highlight the positions that consistently attain high temperatures over this time period. The white/red regions in the standard deviation visualization (Fig. 3d) highlight the positions where temperatures vary significantly across the time period. The visualizations presented in Fig. 4 may be derived for any user-selected range of simulation time span.

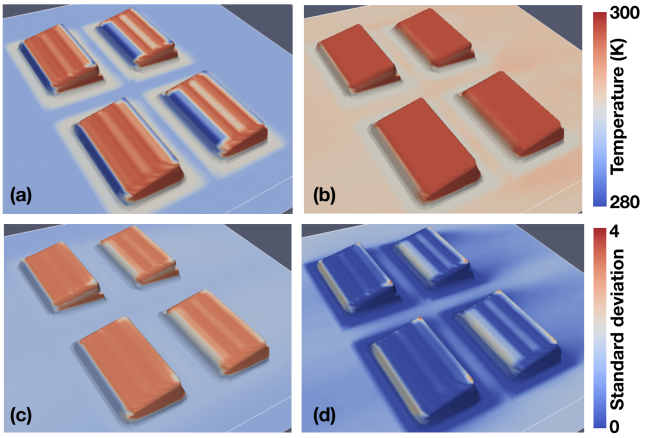

Figure 3: Visualization of the temperature field statistics on solar panel surfaces over the last 11.1 seconds of simulation: (a) minimum, (b) maximum, (c) mean, and (d) standard deviation.

We employ topology-based visualization techniques to gain further insight into the hot and cold spots on the solar panel surfaces. Specifically, we derive critical points and Morse complex segmentation [6] for the temperature field using the topology toolkit [16], as

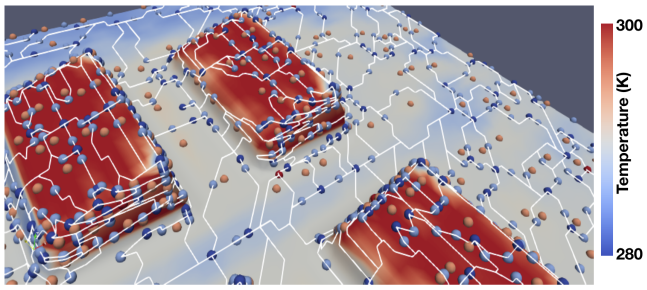

Figure 4: Morse complex visualization of the temperature field on solar panel surfaces at 183.17 minutes in the simulation. The red and dark blue spheres denote local maxima and local minima, respectively. The cool and warm positions on the solar modules are mapped to blue and red, respectively.

visualized in Fig. 4. The red and dark blue spheres denote the positions that exhibit the highest temperature (hot spots) and lowest temperature (cold spots), respectively, in their local neighborhood, where the boundary of the local neighborhood is represented by a Morse complex cell rendered with the white line segments. We present a demo showing how Morse complex segmentation and critical points change with time in an animation[1].

2.2 Visualization of Air Temperature Response to the Heat Source from Solar Panels

We analyze the air temperature variation over time using quartile plots. As observed in the quartile plot shown in Fig. 5, the spatially averaged air temperature increases asymptotically from 280 K to 291.5 K as a result of heat transfer from the solar panels. This plot is generated using ParaView's "Plot Selection over Time" feature, where we select voxels that represent the air.

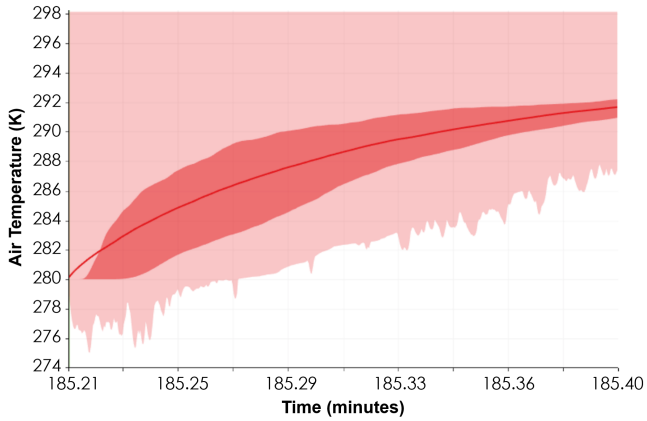

Figure 5: A quartile plot with the solid red line indicating the spatially averaged air temperature, darker red indicating data between Q1 and Q3 (interquartile range), and lighter red indicating data outside the interquartile range.

[1] https://youtu.be/vIDnqXLOcSE

Additionally, we visualize how the solar panel heat is transferred to air particles using streamlines [12] and glyph [2] visualizations in Fig. 1 and via an animation[2]. Specifically, we combine a surface rendering of the solar panels colored by temperature, streamlines to visualize the flow's behavior, and cone glyphs to show the direction of flow. In Fig. 1a, we observe heated air from above the second row soaring upward due to the presence of the solar module. From this visualization, we can easily follow an incoming particle and witness its heat intake as it moves closer to the solar panel.

2.3 Flow Velocity and Eddy Visualizations

We visually investigate flow velocity and eddy formation in the presence of solar panels. In Fig. 6, the streamlines, generated with ParaView's StreamTracer, Tube, and Cone Glyph filters, demonstrate the effects observed in the flow. The color scale shows the higher velocity motions in red and the lower velocities in blue. The higher velocities are found in the upward motions of the flow, and the lower velocities are located just upstream of the solar panels.

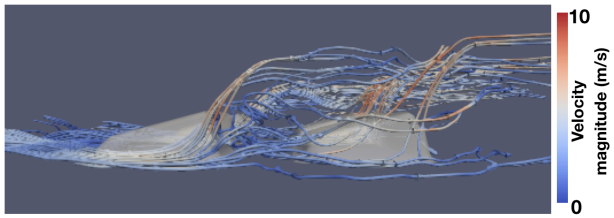

Figure 6: The streamline visualization of the flow field.

Fig. 1b shows a close-up view of Fig. 6 from a different viewpoint to highlight the 3D turbulent motion (indicated by the cyan box) that develops between the two rows of solar panels. A similar eddy formation can also be observed at 185.24 minutes in Fig. 7. Such lateral motions are difficult to capture in 2D visualizations of vertical slices. The solar panel surface temperature is relatively low near the turbulent region of the flow in Fig. 7, as indicated by the cyan box.

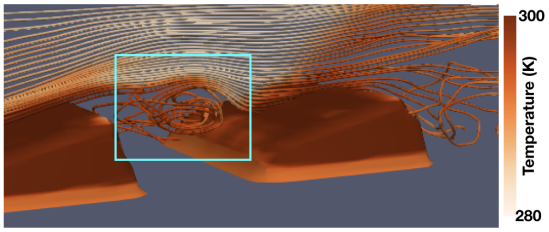

Figure 7: The streamline visualization at 185.24 minutes in the simulation. The solar panel surface temperature appears relatively low near the eddy, as indicated by the cyan box.

Fig. 8 visualizes the velocity magnitude field using direct volume rendering [8]. Direct volume rendering helps extract spatial clusters exhibiting high (Fig. 8a) and low (Fig. 8b) velocities that are not easily observed in streamline visualizations (Fig. 6).

[2] https://www.youtube.com/watch?v=40txQ7lbLBc&t=13s

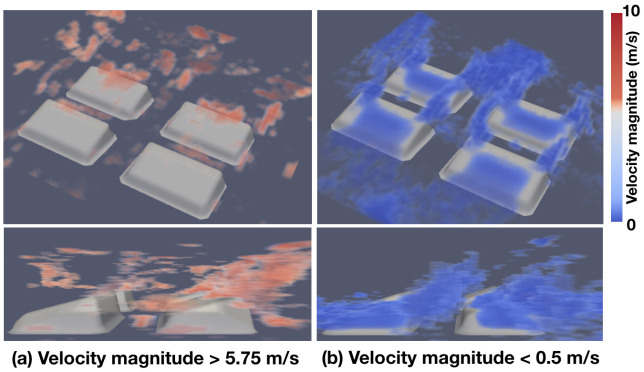

Figure 8: Volume rendering of the velocity magnitude field.

2.4 Visualizations of Heat and Flow Interactions

We employ feature level-sets [9] to study the correlation between velocity magnitude and temperature attributes. Fig. 9a visualizes a scatter plot [7], i.e., the attribute space for the two fields, at 185.32 minutes in the simulation. Overall, the velocity magnitude and temperature fields appear to be negatively correlated from the scatterplot. Fig. 9b visualizes the feature level-sets for the trait representing high temperatures ($\geq 297.5K$) and low velocity magnitudes ($\leq 1m/s$) (the red box in Fig. 9a). The high temperature and low-velocity magnitude regions that match the trait exist on the surface of the rear solar panels, as visualized in dark red. These low-velocity regions result from blockage of the flow by the first row of panels. The high temperature and low-velocity magnitude regions that do not match the trait, but are close to the trait in attribute space, exist on the rear as well as the front solar panel surfaces, as visualized in light red (also see the animation[3]).

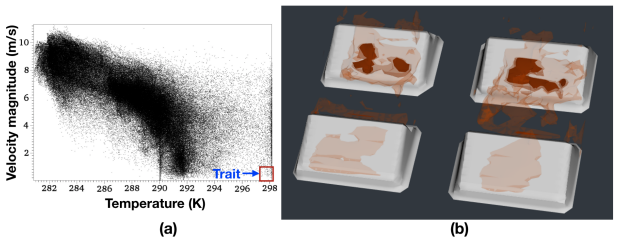

Figure 9: Feature level-sets (b) with high temperatures and low velocities for the trait selected in the scatterplot (a).

Next, we overlay the heat flux and flow variables to study their relationship. Fig. 10 visualizes a heat flux isosurface [10] at 1.5 W/m^2 colored by the temperature and 0.6 opacity combined with flow streamlines colored by the velocity magnitude. From this figure, we observe that the flow tends to carry the heat upward.

Lastly, we visualize the solar panels colormapped with the temperature overlaid with stream ribbons to depict the turbulent behavior just above the panels in Fig. 11 and via an animation[4]. In

[3]https://youtu.be/_08W23AAxV0
[4]https://youtu.be/TAh83x7IK98

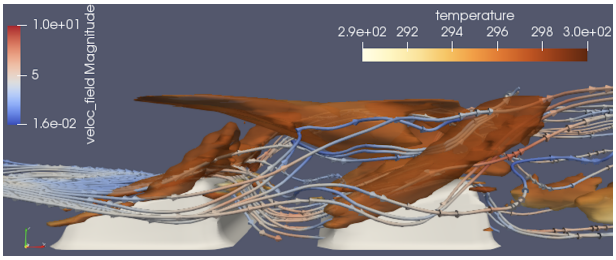

Figure 10: Interplay of flow, represented by streamlines, and heat flux, represented by an isosurface.

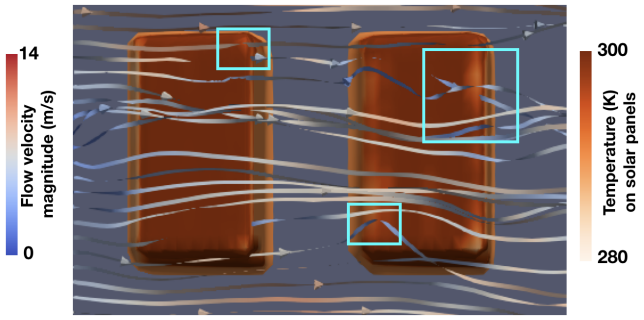

Figure 11: The stream ribbon visualization of flow and vorticity (e.g., ribbon twists inside the cyan boxes) on top of the temperature distributions of solar panels.

Fig. 11, the twisted ribbons denote the vortical regions that appear above the cooler corners of panels, as indicated by the cyan boxes.

3 CONCLUSION AND FUTURE WORK

The visualizations presented herein show how high-quality 3D renderings can significantly complement and add value to 2D plots for the analysis of solar farm LES data. We demonstrate the applications of several 3D visualization techniques, such as streamlines, isosurfaces, direct volume rendering, topology-based visualizations, and feature level-sets, to LES data to study thermal interactions of solar panels with the ABL. Specifically, our proposed visualizations help us gain insight into temperature distributions on solar panels, turbulent motions, heat transfer within ABL flow, and correlations between flow velocities and vortices with solar panel temperatures. Future plans to augment this work include integrating domain expert feedback to further enhance our proposed visualizations and applying these visualizations to high-resolution simulations of non-idealized solar farm geometry.

ACKNOWLEDGMENTS

This work is partially funded by the U.S. Department of Energy [grant number DE-EE0008168] and the Intel Graphics and Visualization Institutes of XeLLENCE. We also acknowledge the Center for High Performance Computing (CHPC) at the University of Utah for computing resources. We would like to thank Dr. Marc Calaf in the Wind, Energy & Turbulence lab at the University of Utah for providing us valuable insights on performing LES for solar farms.

REFERENCES

[1] J. Ahrens, B. Geveci, and C. Law. 2005. *ParaView: An End-User Tool for Large Data Visualization.* Elsevier. 717–731 pages. https://doi.org/10.1016/B978-012387582-2/50038-1

[2] R. Borgo, J. Kehrer, D. H. S. Chung, E. Maguire, R. S. Laramee, H. Hauser, M. Ward, and M. Chen. 2013. Glyph-based Visualization: Foundations, Design Guidelines, Techniques and Applications. In *Eurographics 2013 - State of the Art Reports*, M. Sbert and L. Szirmay-Kalos (Eds.). The Eurographics Association. https://doi.org/10.2312/conf/EG2013/stars/039-063

[3] M. Chamecki, C. Meneveau, and M. B. Parlange. 2008. A hybrid spectral/finite-volume algorithm for large-eddy simulation of scalars in the atmospheric boundary layer. *Boundary-Layer Meteorology* 128, 3 (2008), 473–484. https://doi.org/10.1007/s10546-008-9302-1

[4] H. Childs, E. Brugger, B. Whitlock, and 19 others. 2011. VisIt: An End-User Tool For Visualizing and Analyzing Very Large Data. *Proceedings of SciDAC 2011.*

[5] O. Dupre, R. Vaillon, and M. A. Green. 2017. *Thermal Behavior of Photovoltaic Devices* (1 ed.). Springer International Publishing. https://doi.org/10.1007/978-3-319-49457-9

[6] H. Edelsbrunner, J. Harer, and A. J. Zomorodian. 2003. Hierarchical Morse-Smale Complexes for Piecewise Linear 2-Manifolds. *Discrete and Computational Geometry* 30 (2003), 87–107. https://doi.org/10.1007/s00454-003-2926-5

[7] M. Friendly and D. Denis. 2005. The early origins and development of the scatterplot. *Journal of the History of the Behavioral Sciences* 41, 2 (2005), 103–130. https://doi.org/10.1002/jhbs.20078

[8] M. Hadwiger, J. M. Kniss, C. Rezk-salama, D. Weiskopf, and K. Engel. 2006. *Real-time Volume Graphics.* A. K. Peters, Ltd., Natick, MA, USA.

[9] J. Jankowai and I. Hotz. 2020. Feature Level-Sets: Generalizing Iso-Surfaces to Multi-Variate Data. *IEEE Transactions on Visualization and Computer Graphics* 26, 2 (2020), 1308–1319. https://doi.org/10.1109/TVCG.2018.2867488

[10] W. E. Lorensen and H. E. Cline. 1987. Marching Cubes: A High Resolution 3D Surface Construction Algorithm. *SIGGRAPH Computer Graphics* 21, 4 (1987), 163–169. https://doi.org/10.1145/37402.37422

[11] C. Mohammad and H. Hangan. 2016. A numerical approach to the investigation of wind loading on an array of ground mounted solar photovoltaic (PV) panels. *Jnl. of Wind Engineering and Industrial Aerodynamics* 153 (2016), 60–70. https://doi.org/10.1016/j.jweia.2016.03.009

[12] F. H. Post, B. Vrolijk, H. Hauser, R. S. Laramee, and H. Doleisch. 2002. Feature Extraction and Visualization of Flow Fields. In *Eurographics 2002 - STARs.* Eurographics Association. https://doi.org/10.2312/egst.20021053

[13] S. T. Salesky, M. G. Giometto, M. Chamecki, M. Lehning, and M. B. Parlange. 2019. The transport and deposition of heavy particles in complex terrain: insights from an Eulerian model for large eddy simulation. arXiv:1903.03521 [physics.ao-ph]

[14] W. J. Schroeder, B. Lorensen, and K. Martin. 2004. *The visualization toolkit: an object-oriented approach to 3D graphics.* Kitware. 357–372 pages.

[15] R. Stoll, J. A. Gibbs, S. T. Salesky, W. Anderson, and M. Calaf. 2020. Large-eddy simulation of the atmospheric boundary layer. *Boundary-Layer Meteorology* 177, 2 (2020), 541–581. https://doi.org/10.1007/s10546-020-00556-3

[16] J. Tierny, G. Favelier, J. A. Levine, C. Gueunet, and M. Michaux. 2018. The Topology ToolKit. *IEEE Transactions on Visualization and Computer Graphics* 24, 1 (2018), 832 – 842. https://doi.org/10.1109/TVCG.2017.2743938

[17] J. Wang, P. Van Phuc, Q. Yang, and Y. Tamura. 2020. LES study of wind pressure and flow characteristics of flat-roof-mounted solar arrays. *Journal of Wind Engineering and Industrial Aerodynamics* 198 (2020), 104096. https://doi.org/10.1016/j.jweia.2020.104096